Carbon nanotube superconducting quantum interference device

J.-P. CLEUZIOU[1], W. WERNSDORFER[2]*, V. BOUCHIAT[3], T. ONDARÇUHU[1] AND M. MONTHIOUX[1]

[1]Centre d'Elaboration des Matériaux et d'Etudes Structurales, CEMES-CNRS, 29 rue Jeanne Marvig, 31055 Toulouse Cedex 4, France
[2]Laboratoire L. Néel, LLN-CNRS, associé à l'UJF, BP 166, 38042 Grenoble Cedex 9, France
[3]Centre de Recherches sur les Très Basses Températures, CRTBT-CNRS, associé à l'UJF, BP 166, 38042 Grenoble Cedex 9, France
*e-mail: wolfgang.wernsdorfer@grenoble.cnrs.fr

A superconducting quantum interference device (SQUID) with single-walled carbon nanotube (CNT) Josephson junctions is presented. Quantum confinement in each junction induces a discrete quantum dot (QD) energy level structure, which can be controlled with two lateral electrostatic gates. In addition, a backgate electrode can vary the transparency of the QD barriers, thus permitting change in the hybridization of the QD states with the superconducting contacts. The gates are also used to directly tune the quantum phase interference of the Cooper pairs circulating in the SQUID ring. Optimal modulation of the switching current with magnetic flux is achieved when both QD junctions are in the 'on' or 'off' state. In particular, the SQUID design establishes that these CNT Josephson junctions can be used as gate-controlled π-junctions; that is, the sign of the current–phase relation across the CNT junctions can be tuned with a gate voltage. The CNT-SQUIDs are sensitive local magnetometers, which are very promising for the study of magnetization reversal of an individual magnetic particle or molecule placed on one of the two CNT Josephson junctions.

The superconducting quantum interference device (SQUID) has been used very successfully for magnetometry and voltage or current measurements in the fields of medicine, metrology and other fields of research[1,2]. It combines two quantum properties of superconductivity: the tunnelling of Cooper pairs through a nonsuperconducting medium (the Josephson effect[3]) and flux quantization in a superconducting loop. The direct-current version of this device (DC-SQUID) is composed of a superconducting loop having two Josephson junctions. Its most striking property is that the maximum superconducting current flowing through the device can be periodically modulated by the magnetic flux entering the loop[4], with a period equal to the flux quantum. Recently, miniaturized versions of these devices have been used to implement phase qubits[5] or to measure quantum magnetization reversal of nanoparticles[6] and single-molecule magnets[7].

There has also been enormous progress in the understanding of the electronic and magnetic properties of isolated molecular systems, revealing intriguing new physics. In the early experiments, the measuring devices were composed of two nanoelectrodes and a bridging molecule, allowing the measurement of the electronic transport through single molecules[8]. In such devices, measurements are performed at the molecular level, the observables are referred to molecular orbitals, and not to Bloch waves, as in massive materials. New rules were then found for these systems and it became possible to directly probe the quantum properties of the molecule. For example, the tunnelling of electrons through molecular junctions can show the presence of Coulomb-blockade[8], Kondo coupling[9,10] and shell filling[11], depending on the intensity of coupling between the molecule and the electrodes. Recent progress in improving the contact of CNTs to superconducting nanoelectrodes has shown that such molecules can accommodate a superconducting current[12] and behave as gate-controlled Josephson junctions[13,14]. These CNT junctions are in the quantum-confined regime and can thus act as gate-controlled QDs, that is, devices reminiscent of the well-studied superconducting single-electron transistors[15], but with strong quantum confinement. It was also predicted that a reverse superconducting current (Josephson current) would take place in a junction involving tunnelling through a QD populated with an odd number of electrons[16–21]. Such a junction is also called a π-junction because the spin ordering of the Cooper pair tunnelling through the junction is reversed; that is, the Cooper pair wave function is multiplied by a phase factor $e^{i\pi}$.

We combine here the research area of SQUIDs with that of electronic transport through molecules in order to design a new detector: a SQUID with molecular Josephson junctions made out of CNTs. This system allows us to address the problem of resonant tunnelling through a QD having discrete energy levels and coupled to superconducting electrodes. The SQUID has the advantage of linking the phase across both junctions with the magnetic flux entering the loop. It then yields insight into the current–phase relation across a QD coupled to superconductors. In particular, a gate-controlled transition from the normal to the π-junction can be observed. Owing to the geometrical aspects of CNTs, such SQUIDs are also very promising in the study of spin states of an individual magnetic molecule placed on one of the two CNT Josephson junctions.

RESULTS AND DISCUSSION

SQUID DESIGN AND CNT JUNCTION

We designed and built the first CNT-SQUID as presented in Fig. 1a and described in the Method section. The superconducting SQUID
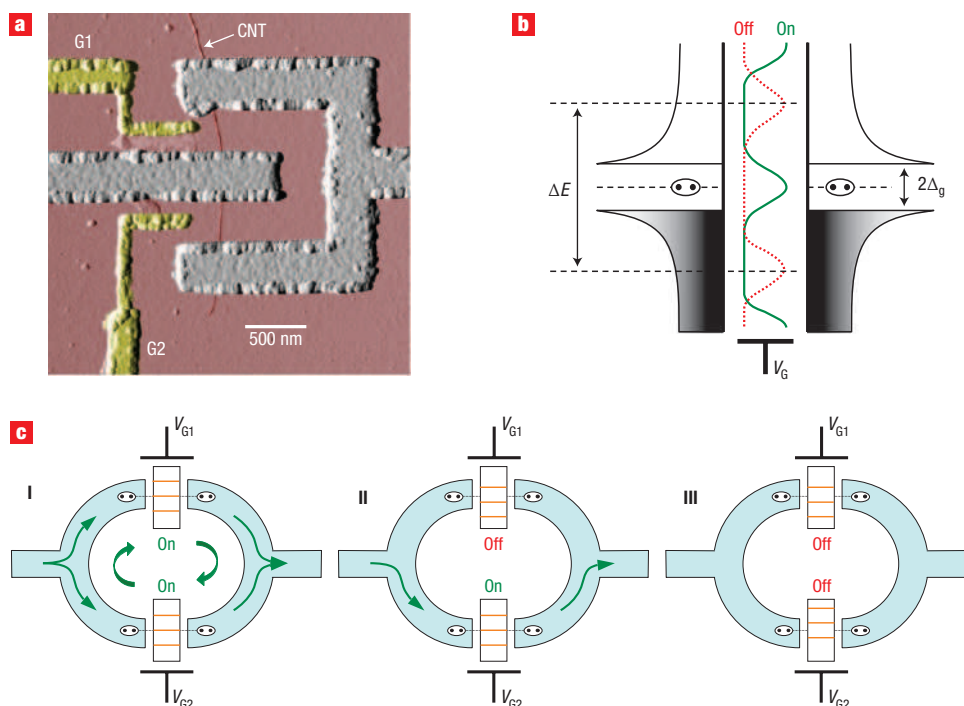
Figure 1 Device and operation scheme. a, Typical device geometry of the CNT-SQUID with two lateral gates G1 and G2 (coloured in gold). The atomic force microscope (AFM) image shows the SQUID loop (grey), which is interrupted by the two CNT Josephson junctions with a length of about 200 nm. The single-walled CNT with a diameter of about 1 nm was located using an AFM, and Pd/Al (3/50 nm) aligned electrodes were deposited over the tube using electron-beam lithography. **b**, Energy level schematics of a QD between two superconducting leads. The energy level spacing ΔE and the superconducting gap $2\Delta_g$ are indicated. The position of the quantum levels can be tuned with a gate voltage V_G. Only when a quantum level is adjusted to the Fermi energies of the superconducting leads (green curve) can a strong supercurrent flow between the leads. **c**, Schematics of the CNT-SQUID with two nanotube junctions, which can be tuned with the gate voltages V_{G1} and V_{G2}. In case **I**, both junctions have a quantum level adjusted to the Fermi energy of the leads (on-resonance) and maximal supercurrent can flow through the device. In cases **II** and **III**, one and two junctions are tuned off-resonance, respectively.

loop is made from Al, and has a critical temperature $T_c \approx 1.2$ K. If not stated differently, all measurements were performed at a cryostat temperature of about 35 mK. The CNT-SQUID contains two CNT-based superconducting transistors, which have been described previously[13,14] and can be modelled by a QD between two superconducting leads (Fig. 1b). The position of the quantum levels can be tuned with gate voltages V_{G1} and V_{G2}. When a quantum level is aligned with respect to the Fermi energy of the superconducting leads ('on' state in Fig. 1b), a supercurrent of a few nanoamperes can flow by resonant tunnelling through the CNT. When the quantum levels are far from the Fermi energy ('off' state in Fig. 1b), the supercurrent is strongly reduced (typically by a factor of 10 to 10^3). However, we show in the following that the supercurrent is not completely suppressed. This effect, not seen before[13], might be due to a Josephson effect via a non-zero electron density between the levels of the CNT and higher-order tunnel processes. Further studies are needed to understand this effect.

ELECTRONIC TRANSPORT PROPERTIES AND KONDO EFFECT

Before turning our attention to the CNT-SQUIDs, we have to characterize the electronic transport properties of our CNT junctions. Particularly important is the interplay between Kondo correlations and superconductivity, which has recently motivated theoretical[16–22] and experimental studies[23–25]. The Kondo correlations are due to a magnetic exchange interaction between a localized magnetic moment and free conduction electrons. In order to minimize the exchange energy, the conduction electrons

tend to screen the magnetic moment and the ensemble forms a spin singlet. It has been predicted that a Kondo resonance in a spin 1/2 QD with an odd electron number can coexist with a superconducting state. Indeed, for strongly hybridized QD states, it has been theoretically predicted[16] that the Josephson coupling could be enhanced by the Kondo resonance. This effect partially offsets the reduction in Josephson coupling due to the Coulomb repulsion energy U_c. The Kondo resonances of each QD can be studied independently by measuring the differential conductance $\mathrm{d}I/\mathrm{d}V$ as a function of source–drain voltage V_{sd} and lateral gate voltage V_G while keeping the chemical potential of the other QD at a constant value. Whereas V_{sd} shifts the Fermi energy of the left lead with respect to the right one, the lateral gate voltage V_G tunes the position of the quantum levels with respect to both Fermi energies of the superconducting leads. The measured conductance map of $\mathrm{d}I/\mathrm{d}V$ versus V_{sd} and V_G exhibits the typical features of Coulomb diamonds (Fig. 2b), which are connected by Kondo 'ridges'[23] of enhanced conductance. The enhanced conductance at zero bias results from the Kondo resonance when there are an odd number of electrons on the QD. Note that the Kondo ridges appear at the same gate voltages as the occurrence of a superconducting state (Fig. 2c). Moreover the maximum supercurrent coincides with the most prominent Kondo ridge (labelled δ in Fig. 2b), a fact that supports the enhancement of superconductivity by the Kondo resonance[16]. The tunnel rate $\Gamma \approx 1$ meV$/h$ (where h is Planck's constant), the Coulomb energy $U_c \approx 6$ meV, and the energy-level spacing $\Delta E \approx 9$ meV are
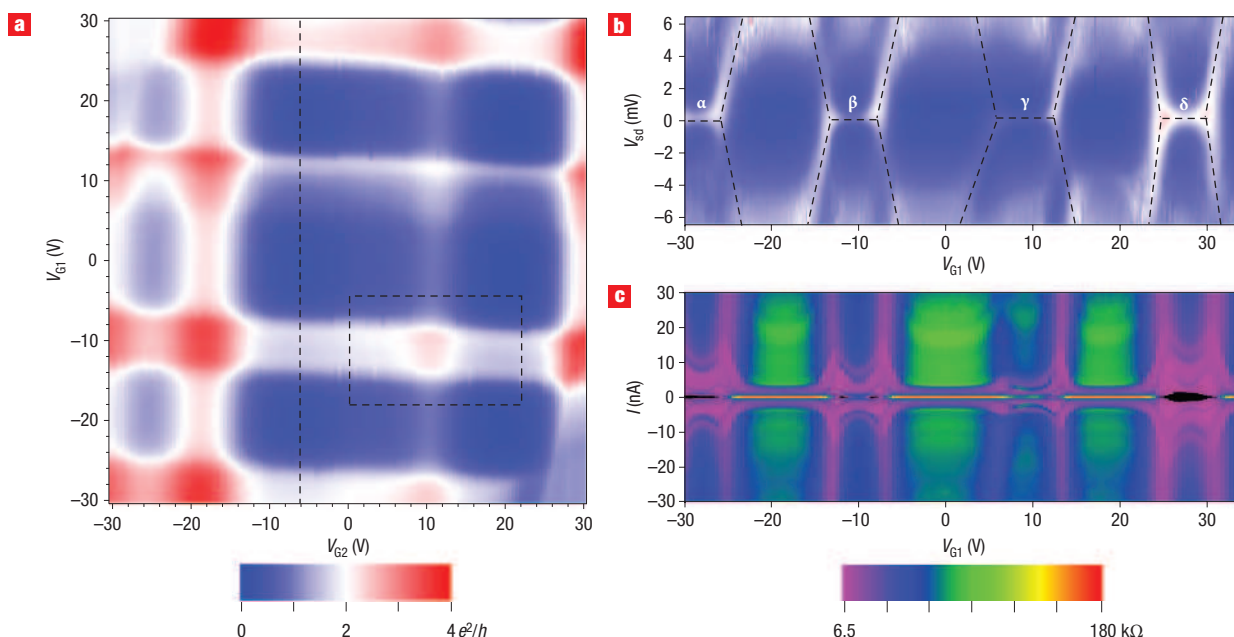
Figure 2 Correlation between Kondo effect and superconductivity. a, Colour-scale representation of a differential conductivity dI/dV map measured at zero bias at 34 mK as a function of the lateral gate voltages V_{G1} and V_{G2} and at a backgate voltage $V_{BG} = 0$ V. A magnetic field of $H_z = 50$ mT was applied perpendicular to the SQUID plane in order to suppress the superconductivity of the leads. The effect of cross-capacitance was subtracted *in situ*. The dotted line indicates the gate voltage range of V_{G1} that is further studied in **b** and **c**, whereas the dotted square encloses the region that is further studied in Fig. 5b and c. **b**, dI/dV map as a function of V_{G1} and source−drain voltage V_{sd}. $V_{G2} = -6$ V and $H_z = 50$ mT. Note that **a** and **b** have the same colour code for dI/dV. The dotted lines in **b** indicate the Coulomb diamonds, which are connected by Kondo ridges labelled α, β, γ and δ. The conductances in the middle of the Kondo ridges are 1.02, 0.72, 0.46 and 1.45 e^2/h for α, β, γ and δ, respectively. (See Supplementary Information for a discussion of the determination of the Kondo temperature.) **c**, Differential resistivity dV/dI map of the same V_{G1} region and for $V_{G2} = -6$ V, but for $H_z = 0$. A supercurrent is observed in the black regions, which correspond to the Kondo ridges in **b**.
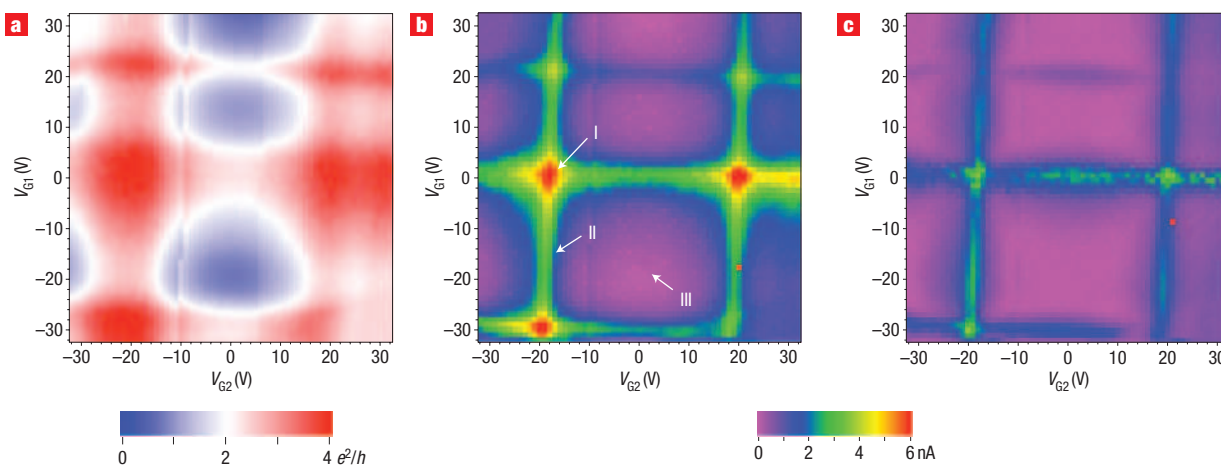

Figure 3 Correlation between normal-state conductance and superconducting switching current. a, Colour-scale representation of a typical differential conductivity dI/dV map at 34 mK and a backgate voltage $V_{BG} = -6$ V as a function of the lateral gate voltages V_{G1} and V_{G2}. A magnetic field of $H_z = 50$ mT was applied perpendicular to the SQUID plane in order to suppress the superconductivity of the leads. The effect of cross-capacitance was subtracted *in situ*. **b,c**, Colour-scale representations of the switching current I_{sw} at 30 mK as a function of V_{G1} and V_{G2} at the same backgate voltage. Magnetic fields $H_z = 0$ and 1.3 mT were applied in **b** and **c**, respectively. The latter corresponds to half a flux quantum ($h/4e$). I_{sw} is maximal or minimal when both junctions are tuned on- or off-resonance, respectively (the three cases I, II and III of Fig. 1c are indicated). Each pixel corresponds to a single measurement of I_{sw}.

obtained from the size and shape of the Coulomb diamonds. Using $\Delta E = h\nu_F/2kL$, where $\nu_F = 8.1 \times 10^5$ m s^{-1} is the Fermi velocity in the CNT, $k = 1$ for orbital and spin degeneracies, $k = 2$ for only spin degeneracy, and L is the length of the CNT. We obtained $L = 186$ nm for $k = 1$, which is in agreement with the length of 200 nm estimated using atomic force microscopy

(AFM). This suggests that our CNTs have orbital and spin degeneracies. However, the gate dependence does not exhibit a clear fourfold symmetry as expected for such degenerate QDs[11] but rather an even–odd behaviour[26], which may have two origins. First, channel mixing might occur at the transparent contacts. More probable, however, is the influence of defects induced either by the interaction of the CNT with the substrate, or by structural imperfections inside the nanotube. These defects lower the symmetry of the system and thereby lift the orbital degeneracy[27].

CNT-SQUID CHARACTERISTICS

The operation of the CNT-SQUID is based on the quantum phase interference of the supercurrent flowing through two CNT-based superconducting transistors[13] in a superconducting ring (Fig. 1c). The position of the quantum levels in each junction can be individually tuned using the two lateral gate voltages V_{G1} and V_{G2}, and the transparency of the CNT contact barriers can be globally adjusted using the backgate voltage V_{BG}.

In order to find the gate voltages required to adjust the levels of each CNT junction with respect to the Fermi energy of their contacts, we measured the differential conductance dI/dV at zero bias as a function of V_{G1}, V_{G2} and V_{BG} in a field of $H_z = 50$ mT to drive the superconducting leads to the normal state (Figs. 2a and 3a). The maps follow the stability diagram of two QDs in parallel, that is, a chequerboard pattern with high-conductance states having values of the order $4e^2/h$ (where e^2/h is the conductance quantum) centred on points where both CNTs are on-resonance, and low-conductance states (typically between 0.1 and 0.5 e^2/h), where both CNTs are off-resonance.

At small applied fields, the CNT junctions transmit a supercurrent. We define the switching current I_{sw} as the maximum dissipationless current that the Josephson junctions can pass through the device. I_{sw} is measured by ramping the current at a constant sweep rate from zero to I_{sw}, at which point a voltage drop is measured across the junction. Fig. 3b,c presents I_{sw} as a function of V_{G1} and V_{G2} in zero field and in a perpendicular magnetic field $H_z = 1.3$ mT corresponding to a magnetic flux, penetrating the SQUID loop, of $\Phi_e = \Phi_0/2 = h/4e$ where Φ_0 is the magnetic flux quantum. Comparing the dI/dV map (Fig. 3a) with the I_{sw} map (Fig. 3b,c) shows that I_{sw} is maximal (about 6 nA) at maximal conductance in the normal state, that is, when both CNTs are on-resonance. I_{sw} is about two times smaller when only one CNT is on-resonance. Typical voltage versus current characteristics and field modulations of I_{sw} are presented in Fig. 4. The overall flux modulation of the CNT-SQUID can be understood by using a standard SQUID model[2], which predicts the field dependence of the maximal supercurrent, called the critical current I_c:

$$I_c = \sqrt{(I_{c1} - I_{c2})^2 + 4I_{c1}I_{c2}\cos^2(\pi\,\Phi_e/\Phi_0)} \qquad (1)$$

Here, I_{ci} are the critical currents of each Josephson junction ($i = 1$ and 2), which can be tuned independently with the gate voltages V_{G1} and V_{G2}. I_c is an upper bound of the experimentally observed switching current I_{sw}, because the former neglects environmental effects like temperature, electronic noise and quantum effects. The field modulation depth is maximal when I_{c1} and I_{c2} are comparable (Figs. 3 and 4), but it is minimal when the difference between both current magnitudes is maximal. For short junctions, the maximal supercurrent at zero temperature for a single-channel junction is given by $I_{ci} = e\Delta_g/\hbar$, where $2\Delta_g$ is the superconducting gap and $\hbar$ is the reduced Planck constant.
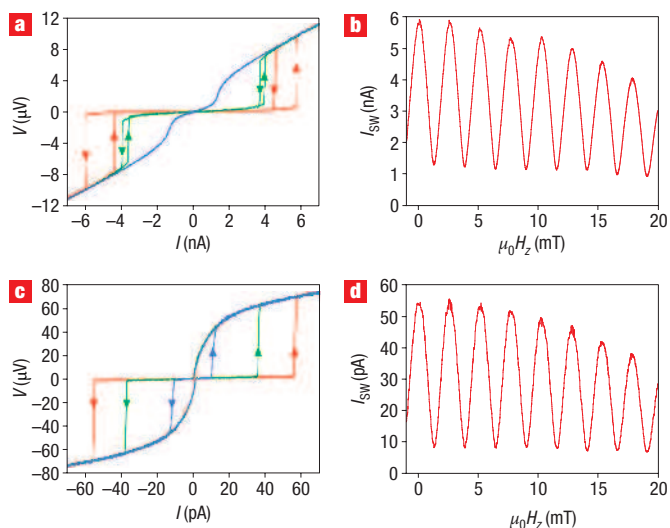
Figure 4 CNT-SQUID characteristics. a,c, Voltage versus current curves at three applied fields corresponding to zero (red), a quarter (green) and a half (blue) flux quantum for the situations when both junctions are tuned on-resonance (**a**) or off-resonance (**c**) **a** and **c** correspond to maximal and minimal switching currents in Figs. 3b and 2a, respectively. The current was swept at sweep rates of 0.5 nA s^{-1} and 5 pA s^{-1} for **a** and **c**, respectively. Note that each curve is a single sweep (no data averaging was performed). **b,d,** Field modulation of the switching current I_{sw} for the situations in **a** and **c**, respectively. Each point in **b** and **d** corresponds to a single measurement taken at frequencies of 1 and 0.1 Hz, respectively. The field periodicity times the area of the SQUID loop is in good agreement with a flux quantum ($h/2e$).

Because of proximity effects between the Al and the Pd contact layers, the effective gap of the contacting bilayer is reduced to $2\Delta_g \approx 0.12$ meV (data extracted from the temperature dependence of $dI/dV(T)$; see Supplementary Information). We yield $I_{ci} = 15$ nA, which is further reduced when the asymmetry of the barrier is taken into account[28]. Experimentally, we do not measure I_{ci}, but a maximal switching current $I_{sw} \approx 3$ nA per junction for the device presented here. The highest value achieved so far with our single-walled CNT junction is $I_{sw} \approx 5$ nA. The discrepancy between I_{ci} and I_{sw} is due to the fact that the latter is a stochastic variable influenced by temperature, electronic noise and quantum effects. The effect of the electromagnetic environment can drastically reduce I_{sw}, especially for small, underdamped, current-biased Josephson junctions[29]. Another manifestation of the electromagnetic environment is that the superconducting branch exhibits a small bending towards a non-zero voltage (Fig. 4a,c) due to retrapping effects[30].

CNT π-JUNCTION

A closer investigation of the field modulation shows strong deviations from equation (1). In particular, when the contact barriers are increased with the backgate voltage, a reduced Kondo effect is found (see Supplementary Information) and, under certain gate voltages, the contrast of the interference fringes drops to zero and finally exhibits a phase shift, leading to a minimum switching current at zero field (Fig. 5). Such an effect, in which the minimum energy state of one of the Josephson junctions (the so-called π-junction) is obtained for a phase difference of π instead of zero, has been the object of intense studies in the past decade. It has been reported experimentally as a consequence of d-wave superconductivity[31],
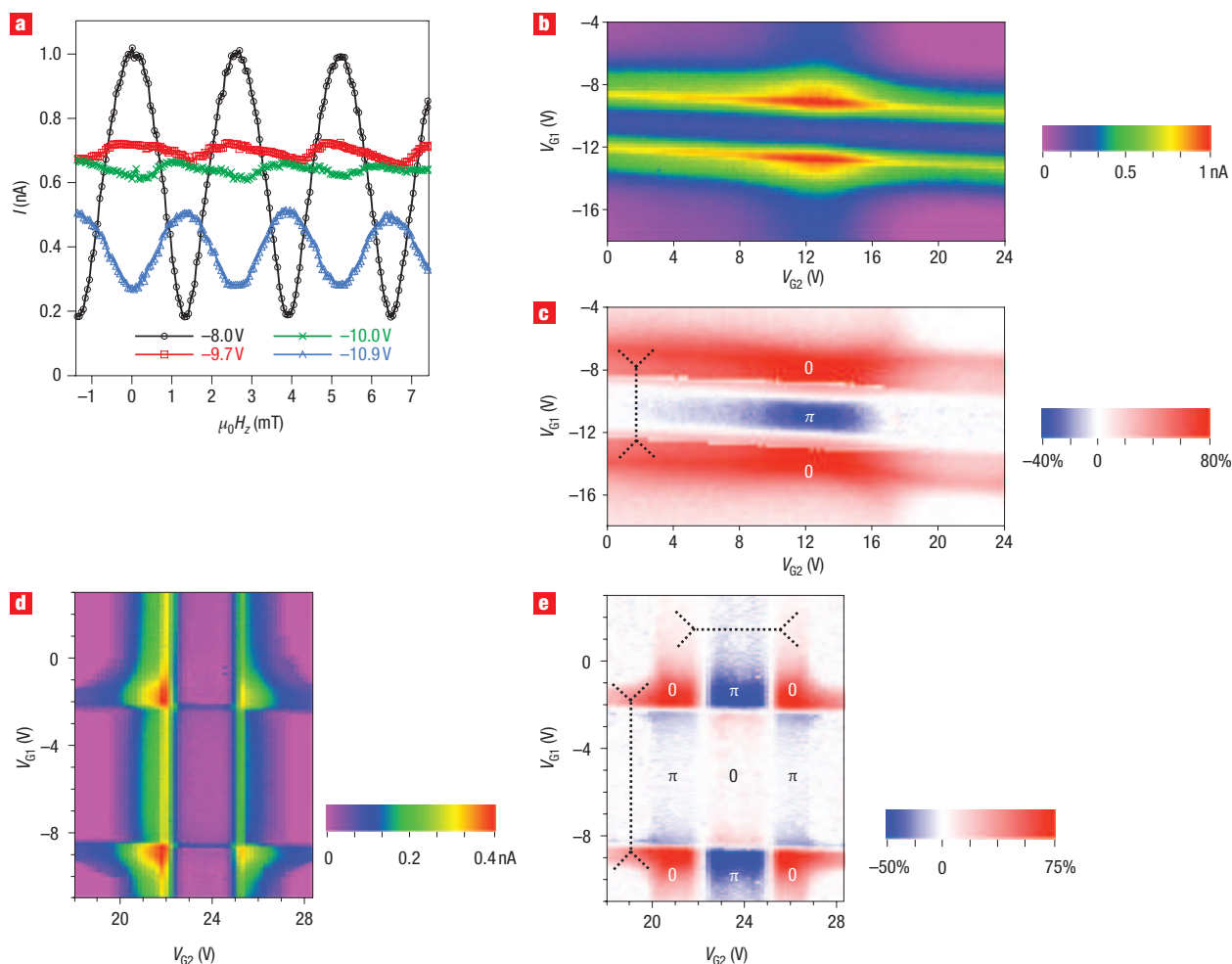
Figure 5 Gate-controlled π-junction CNT-SQUID characteristics. a, Field modulation of the switching current I_{sw} for a grounded backgate ($V_{BG} = 0$ V), where a weak Kondo coupling was observed. Using the lateral gate voltage V_{G1} while keeping the gate voltage V_{G2} at 12.5 V, the flux modulation can be driven from an even (0-junction SQUID, black) to an odd (π-junction SQUID, blue) curve. In the vicinity of the phase reversal, the field modulation exhibits a clear distortion from a sine dependence, suggesting a peculiar current phase relation in that case. Each point corresponds to a single I_{sw} measurement (no averaging). **b–e**, Colour-scale representations of the maximum switching current I_{sw} (**b** and **d**) and normalized field modulation maps (**c** and **e**) as a function of the lateral gate voltages V_{G1} and V_{G2} for two different backgate voltages $V_{BG} = 0$ (**a** and **b**) and 1 V (**d** and **e**). Each pixel corresponds to a single measurement of I_{sw}. The V_{G1}–V_{G2} zone in **b** and **c** is indicated by the dotted square in Fig. 2a. Red and blue regions in **c** and **e** correspond to even (0) and odd (π) flux modulation, respectively. **b**,**c** and **d**,**e** show the situations when only one or two junctions are tuned via a π-transition, respectively. Note that in the centre of **e**, both junctions have a π-shift, leading to an even flux modulation. The sizes and positions of the corresponding Kondo ridges in the normal state (see Supplementary Information) are schematically indicated by dotted lines in **c** and **e**.

when tunnelling occurs through a ferromagnetic layer[32,33]. Local control of the sign of a Josephson current was also proved possible[34] by tuning the local density of state of an SNS junction[35]. Reminiscent of a ferromagnetic impurity in a Josephson junction, it was predicted that a reverse Josephson current would take place in a junction involving tunnelling through a QD populated with an odd number of electrons[16–21]. For a strong Kondo effect (Fig. 3), the Josephson coupling is expected to be positive (0-junction) because the localized spin is screened due to the Kondo effect. On the other hand, for a weak Kondo effect (Fig. 5), the large on-site interaction only allows the electrons in a Cooper pair to tunnel one by one via virtual processes in which the spin ordering of the Cooper pair is reversed, leading to a negative Josephson coupling (π-junction).

This prediction can be demonstrated with our CNT-SQUID because it links the phase across both junctions to the magnetic flux entering the loop. When one of the two junctions has a negative Josephson coupling, the flux modulation is odd, that is, I_{sw} has a minimum at zero field. However, when both junctions have a positive or a negative Josephson coupling, the flux modulation is even, that is, I_{sw} has a maximum at zero field. Because the number of electrons in the QD is odd in the middle of a Kondo ridge and even at the outside, a gate voltage allows us to vary the QD junction from a positive to a negative Josephson coupling. Fig. 5 details the situations when only one (Fig. 5b,c) or two (Fig. 5d,e) junctions are tuned via a π-transition. Such CNT devices are therefore very promising in circumstances where gate-controlled phase-relations are needed. For example, theoretical works have shown that a π-Josephson junction has a

protection against decoherence[36]. Consequently, a π-junction SQUID can be well suited to implementing a qubit with a long coherence time[37].

PROSPECTS FOR DETECTING SINGLE MAGNETIC MOMENTS

In designing a CNT-SQUID, our motivation is to use it as a detector for magnetization switching of the magnetic moment of a single molecule. The aspect ratio of CNTs makes them ideal for coupling to single nanometre-sized objects. For example, it has been shown that a semiconducting nanotube properly functionalized and operated at the conduction threshold has the ability to sense the binding of a single molecule by electrostatic coupling[38]. In this paper, we present a device that we want to use to detect the switching of few magnetic moments. Indeed, SQUIDs are the most sensitive magnetic flux detectors[2,39]. The magnetic flux variation $\Delta\Phi$ is related to the magnetization change ΔM associated with the reversal of magnetic moments: $\Delta\Phi = \alpha\Delta M$, where α is the flux coupling factor determined by the geometry of the device and the sample. The flux sensitivity of a SQUID is limited by the quantum limit, which has been achieved experimentally by several groups[2,40]. However, the high sensitivity of such SQUIDs cannot be used to detect the magnetization reversal of single nanoparticles or molecules because of the very small flux coupling factor α. An improvement was achieved with planar microbridge DC-SQUIDs (Fig. 6a). A 3-nm particle was placed on top of a microbridge with a cross-section of 50×20 nm^2 (Fig. 6b). The coupling was strong enough to study 10^3 magnetic moments[41,42]. However, the flux coupling factor was rather poor (Fig. 6b). In the case of a CNT junction (Fig. 6c), a nanometre-sized molecule could be placed directly on the CNT, which has a cross-section of about 1 nm^2. We therefore expect a nearly optimized coupling factor α, because the molecule size and the junction cross-section are comparable (Fig. 6d). The precise calculation of α is difficult in such a near-field situation for which the dipolar approximation is not valid. However, a rough estimate of the magnetic signal of a Mn$_{12}$ molecule, sitting on the CNT, yields a flux variation of 10^{-4} flux quantum, which should be within the sensitivity of our measurements (see Supporting Information for the first estimation of the flux sensitivity of CNT-SQUIDs).

In order to detect rapidly the switching of magnetization, we often use the SQUID as a threshold detector[41,42]. This method, called the cold mode, consists in biasing the SQUID close to the switching current. The magnetization reversal triggers a transition of the SQUID from the superconducting to the normal state because of the fast magnetization change and/or the associated dissipation. A dV/dt pulse can then be easily detected on the current lead biasing the SQUID because of the hysteretic behaviour of the SQUID. The sensitivity of the cold mode scales roughly with the inverse of the switching current; we therefore expect a strong improvement with the CNT-SQUIDs, which have a tunable switching current in the nano and picoampere regions instead of the microampere region of previous SQUIDs[41,42].

Another important feature of the CNT-SQUIDs concerns the ability to tune the coupling between the detector and sample. Indeed, the supercurrent through the junction can be switched on and off using the lateral gate. In the off state, the magnetic molecule is decoupled from the measuring device and it can evolve without decoherence coming from the device. In order to measure the magnetization state of the molecule, the SQUID is then switched on. This should have important consequences as it allows us to limit the back-action of the CNT-SQUID on the quantum state of a single molecule magnet.
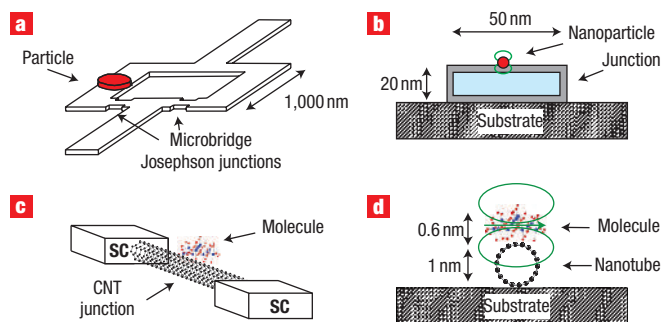

Figure 6 Schematics of single-molecule studies using CNT-SQUIDs.
a, Schematic of a planar microbridge DC-SQUID on which a ferromagnetic particle is placed. The SQUID detects the flux through its loop, produced by the sample magnetization. **b**, Cross-section (50×20 nm^2) of a microbridge junction on which a 3-nm particle is placed. The magnetic field lines are shown in green. The flux coupling is poor because of the large mismatch between the particle size and the junction cross-section. **c**, Schematic of one of the two junctions of a CNT-SQUID separating the superconducting (SC) leads. A nanometre-sized molecule sits on top of the CNT. **d**, Cross-section (1 nm^2) of a CNT junction on which a 0.6-nm molecule is placed. The flux coupling is optimized because the molecule size and the junction cross-section are comparable.

Further improvement of the flux sensitivity could be achieved with a new readout scheme, which probes the SQUID's nonlinear inductance rather than its resistance[43]. The SQUID is driven with a microwave frequency a.c. current near a bifurcation point where two oscillation states exist[44]. These superconducting dynamical states differ in amplitude and phase, and are associated with zero d.c. voltage. They can be distinguished by measuring a change in amplitude or phase of the a.c. voltage across the SQUID[43]. In this non-dissipative, dispersive SQUID magnetometer, the switching from one dynamical state to the other would signal a change in spin state of the molecule. As the working temperature of our devices was limited to a few hundred millikelvin, further improvements could be achieved by using other superconducting materials with higher T_c, such as Nb, Sn and NbTi.

In conclusion, the CNT-SQUIDs provide a new generation of ultrasensitive magnetometers of nanometre-sized samples. Such devices also offer the opportunity to test interesting physical phenomena ranging from Kondo physics to π-junctions, and pave the way for non-locality experiments by generating pairs of entangled electrons in a nanotube[45–47].

METHODS

In order to build a CNT-SQUID as presented in Fig. 1a, we started from a degenerately n-doped silicon substrate with a 350-nm-thick thermally grown SiO$_2$ layer on top, which was used as a backgate. Single-walled CNTs were prepared by the laser vaporization method[48] at Rice University. They were dispersed in water by sonication using sodium dodecyl sulphate as surfactant. The CNTs were deposited using a combing technique, which allows good control of the CNT density and orientation on the substrate[49]. The silica surface was first functionalized using a standard silanization technique, leading to a self-assembled monolayer of aminopropyltriethoxysilane (Aldrich). The substrate was then dipped for 5 min in the dispersion of CNTs and withdrawn at a constant velocity of 200 μm s^{-1}. The sample was thoroughly washed in distilled water in order to remove the surfactant from the nanotubes. The nanotube location was imaged by AFM, and aligned e-beam lithography was carried out to pattern the SQUID loops and the contacts. The fork geometry for the loop allowed us to fabricate both junctions from the same nanotube. Metal electrodes

were deposited using electron-gun evaporation and a thickness of 3 nm Pd followed by 50 nm Al was used. Pd provides high-transparency contacts to the CNTs[50]. Al is a superconductor widely used in nanoscale devices, having a critical temperature of about 1.2 K. Only devices with resistance below 30 kΩ and no significant gate effect at room temperature were used for our studies. In addition to the backgate, two lateral gates G1 and G2 were aligned to each device, allowing us to tune independently the electronic properties of each CNT junction (Fig. 1a).

We fabricated about 100 CNT-SQUIDs and 300 CNT superconducting transistors using CNTs, ropes of CNTs and multiwalled CNTs. Only devices having individual CNTs are presented here. About 30% of all devices worked similarly to the presented one. Fabrication failure was caused mainly because of misalignment of the contact pads and lateral gates, low-conductance nanotube−metal contacts, and semiconducting CNTs. The properties of the superconducting contacts, and our filtering system are discussed in the Supplementary Information.

References

1. Clarke, J., Cleland, A. N., Devoret, M. H., Esteve, D. & Martinis, J. M. Quantum mechanics of a macroscopic variable: the phase difference of a Josephson junction. *Science* **239**, 992−997 (1988).
2. Clarke, J. & Braginski, A. I. (eds) *The SQUID Handbook* (Wiley-VCH, Weinheim, 2004).
3. Josephson, B. D. Possible new effects in superconductive tunnelling. *Phys. Lett.* **1**, 251−253 (1962).
4. Jaklevic, R. C., Lambe, J., Silver, A. H. & Mercereau, J. E. Quantum interference effects in Josephson tunneling. *Phys. Rev. Lett.* **12**, 159−160 (1964).
5. Chiorescu, I., Nakamura, Y., Harmans, C. J. P. M. & Mooij, J. E. Coherent quantum dynamics of a superconducting flux qubit. *Science* **299**, 1869−1871 (2003).
6. Wernsdorfer, W. *et al.* Macroscopic quantum tunneling of magnetization of single ferrimagnetic nanoparticles of barium ferrite. *Phys. Rev. Lett.* **79**, 4014−4017 (1997).
7. Wernsdorfer, W. & Sessoli, R. Quantum phase interference and parity effects in magnetic molecular clusters. *Science* **284**, 133−135 (1999).
8. Tans, S. J. *et al.* Individual single-wall carbon nanotubes as quantum wires. *Nature* **386**, 474−477 (1997).
9. Nygard, J., Cobden, D. H. & Lindelof, P. E. Kondo physics in carbon nanotubes. *Nature* **408**, 342−346 (2000).
10. Park, J. *et al.* Coulomb blockade and the Kondo effect in single-atom transistors. *Nature* **417**, 722−725 (2002).
11. Liang, W., Bockrath, M. & Park, H. Shell filling and exchange coupling in metallic single-walled carbon nanotubes. *Phys. Rev. Lett.* **88**, 126801 (2002).
12. Kasumov, A. Y. *et al.* Supercurrents through single-walled carbon nanotubes. *Science* **397**, 598−601 (1999).
13. Jarillo-Herrero, P., van Dam, J. A. & Kouwenhoven, L. P. Quantum supercurrent transistors in carbon nanotubes. *Nature* **439**, 953−956 (2006).
14. Jørgensen, H. I., Grove-Rasmussen, K., Novotn, T., Flensberg, K. & Lindelof, P. E. Electron transport in single-wall carbon nanotube weak links in the Fabry-Perot regime. *Phys. Rev. Lett.* **96**, 207003 (2006).
15. Joyez, P. The Single Cooper Pair Transistor: A Macroscopic Quantum Device. Thesis, Univ. Paris 6 (1995); available at http://www.drecam/cea.fr
16. Glazman, L. I. & Matveev, K. A. Resonant Josephson current through Kondo impurities in a tunnel barrier. *JETP Lett.* **49**, 659−662 (1989).
17. Levy Yeyati, A., Cuevas, J. C., Lopez-Davalos, A. & Martin-Rodero, A. Resonant tunneling through a small quantum dot coupled to superconducting leads. *Phys. Rev. B* **55**, 6137−6140 (1997).
18. Rozhkov, A. V., Arovas, D. P. & Guinea, F. Josephson coupling through a quantum dot. *Phys. Rev. B* **64**, 233301 (2001).
19. Zaikin, A. D. Some novel effects in superconducting nanojunctions. *Low Temp. Phys.* **30**, 568−578 (2004).
20. Siano, F. & Egger, R. Josephson current through a nanoscale magnetic quantum dot. *Phys. Rev. Lett.* **93**, 047002 (2004).
21. Choi, M. S., Lee, M., Kang, K. & Belzig, W. Kondo effect and Josephson current through a quantum dot between two superconductors. *Phys. Rev. B* **70**, 020502 (2004).
22. Kouwenhoven, L. & Glazman, L. Revival of the Kondo effect. *Phys. World* **14**, 33−38 (January 2001).
23. Goldhaber-Gordon, D. *et al.* Kondo effect in a single-electron transistor. *Nature* **391**, 156−159 (1998).
24. Buitelaar, M. R., Nussbaumer, T. & Schonenberger, C. Quantum dot in the Kondo regime coupled to superconductors. *Phys. Rev. Lett.* **89**, 256801 (2002).
25. Buitelaar, M. R. *et al.* Multiple Andreev reflections in a carbon nanotube quantum dot. *Phys. Rev. Lett.* **91**, 057005 (2003).
26. Cobden, D. H. & Nygard, J. Shell filling in closed single-wall carbon nanotube quantum dots. *Phys. Rev. Lett.* **89**, 046803 (2002).
27. Ke, S.-H., Baranger, H. U. & Yang, W. Addition energies of fullerenes and carbon nanotubes as quantum dots: the role of symmetry. *Phys. Rev. Lett.* **91**, 116803 (2003).
28. Beenakker, C. W. J. & van Houten, H. *Single-electron Tunneling and Mesoscopic Devices* (eds Koch, H. & Lübbig, H.) 175−179 (Springer, Berlin, 1992); ibid. <http://xxx.lanl.gov/abs/condmat/0111505l> (2001).
29. Joyez, P., Lafarge, P., Filipe, A., Esteve, D. & Devoret, M. H. Observation of parity-induced suppression of Josephson tunneling in the superconducting single-electron transistor. *Phys. Rev. Lett.* **72**, 2458−2461 (1994).
30. Vion, D., Götz, M., Joyez, P., Esteve, D. & Devoret, M. H. Thermal activation above a dissipation barrier: switching of a small Josephson junction. *Phys. Rev. Lett.* **77**, 3435−3438 (1996).
31. Schulz, R. R. *et al.* Design and realization of an all d-wave dc π-superconducting quantum interference device. *Appl. Phys. Lett.* **76**, 912−914 (2000).
32. Kontos, T. *et al.* Josephson junction through a thin ferromagnetic layer: negative coupling. *Phys. Rev. Lett.* **89**, 137007 (2002).
33. Guichard, W. *et al.* Phase sensitive experiments in ferromagnetic-based Josephson junctions. *Phys. Rev. Lett.* **90**, 167001 (2003).
34. Baselmans, J. J. A., van Wees, B. J. & Klapwijk, T. M. Controllable π-SQUID. *Appl. Phys. Lett.* **79**, 2940−2942 (2001).
35. Baselmans, J. J. A., Morpurgo, A. F., van Wees, B. J. & Klapwijk, T. M. Reversing the direction of the supercurrent in a controllable Josephson junction. *Nature* **397**, 43−45 (1999).
36. Ioffe, L. B., Geshkenbein, V. B., Feigel'man, M. V., Fauchere, A. L. & Blatter, G. Environmentally decoupled sds-wave Josephson junctions for quantum computing. *Nature* **398**, 679−681 (1999).
37. Yamashita, T., Tanikawa, K., Takahashi, S. & Maekawa, S. Superconducting qubit with a ferromagnetic Josephson junction. *Phys. Rev. Lett.* **95**, 097001 (2005).
38. Besteman, K., Lee, J. O., Wiertz, F. G. M., Heering, H. A. & Dekker, C. Enzyme-coated carbon nanotubes as single-molecule biosensors. *Nano Lett.* **3**, 727−730 (2003).
39. Ketchen, M. B. & Kirtley, J. R. Design and performance aspects of pickup loop structures for miniature SQUID magnetometry. *IEEE Appl. Supercond.* **5**, 2133−2136 (1995).
40. Mück, M., Welzel, C. & Clarke, J. Superconducting quantum interference device amplifiers at gigahertz frequencies. *Appl. Phys. Lett.* **82**, 3266−3268 (2003).
41. Wernsdorfer, W. Classical and quantum magnetization reversal studies in nanometer-sized particles and clusters. *Adv. Chem. Phys.* **188**, 99−190 (2001).
42. Jamet, M. *et al.* Magnetic anisotropy of a single cobalt nanocluster. *Phys. Rev. Lett.* **86**, 4676−4679 (2001).
43. Siddiqi, I. *et al.* RF-driven Josephson bifurcation amplifier for quantum measurement. *Phys. Rev. Lett.* **93**, 207002 (2004).
44. Siddiqi, I. *et al.* Direct observation of dynamical bifurcation between two driven oscillation states of a Josephson junction. *Phys. Rev. Lett.* **94**, 027005 (2005).
45. Recher, P. & Loss, D. Superconductor coupled to two Luttinger liquids as an entangler for electron spins. *Phys. Rev. B* **65**, 165327 (2002).
46. Bena, C., Vishveshwara, S., Balents, L. & Fisher, M. P. A. Quantum entanglement in carbon nanotubes. *Phys. Rev. Lett.* **89**, 037901 (2002).
47. Bouchiat, V. *et al.* Single-walled carbon nanotube−superconductor entangler: noise correlations and Einstein−Podolsky−Rosen states. *Nanotechnology* **14**, 77−85 (2003).
48. Thess, A. *et al.* Crystalline ropes of metallic carbon nanotubes. *Science* **273**, 483−485 (1996).
49. Gerdes, S., Ondarcuhu, T., Cholet, S. & Joachim, C. Combing a carbon nanotube on a flat metal−insulator−metal nanojunction. *Europhys. Lett.* **48**, 292−298 (1999).
50. Javey, A., Guo, J.,Wang, Q., Lundstrom, M. & Dai, H. Ballistic carbon nanotube field-effect transistors. *Nature* **424**, 654−657 (2003).

Author contributions

J.-P.C. fabricated the devices, and W.W. conceived and performed the experiments with help from J.-P.C. and V.B. All authors discussed the results and commented on the manuscript.

Competing financial interests

The authors declare that they have no competing financial interests.